frontiers in Materials

ORIGINAL RESEARCH
published: 04 February 2019
doi: 10.3389/fmats.2019.00005

Citric Acid Modified Bentonite for Congo Red Adsorption

Hanbing Zhang[1,2], *Juan Zhou*[2,3], *Yaseen Muhammad*[2,4], *Rui Tang*[2], *Kun Liu*[1], *Ying Zhu*[1] *and Zhangfa Tong*[2*]

[1] Institute of Environmental Engineering, College of Resources, Environment and Materials, Guangxi University, Nanning, China, [2] Guangxi Key Laboratory of Petrochemical Resource Processing and Process Intensification Technology, School of Chemistry and Chemical Engineering, Guangxi University, Nanning, China, [3] Guangzhou of China Light Industry Engineering Co. Ltd., Guangzhou, China, [4] Institute of Chemical Sciences, University of Peshawar, Peshawar, Pakistan

Raw bentonite (RB) was chemically modified by citric acid (CA) to obtain a low-cost and environment-friendly citric acid incorporated bentonite (CAB) adsorbent, which was applied for the adsorptive removal of Congo Red (CR). The effect of adsorbent dosage, contact time, ionic strength, surfactant, and pH on adsorption was investigated. Adsorption equilibrium data fitted well with Langmuir model while the Langmuir adsorption capacity of CR on CAB reached up to 384 $mg{\cdot}g^{-1}$. Furthermore, CR adsorption on CAB followed pseudo-second kinetic model while intra-particle diffusion was not the only rate-limiting step as determined from intra-particle diffusion model investigation. RB and CAB were characterized by XRD, FT-IR, and BET techniques. A proposed mechanism for the adsorption of CR over CAB suggested the chemical adsorption phenomenon is mainly controlled by chelation, hydrogen bonding, and fixing.

Keywords: citric acid modified bentonite, Congo Red, adsorption model, adsorption mechanism, XRD and FT-IR

OPEN ACCESS

Edited by:
Jie-Sheng Chen,
Shanghai Jiao Tong University, China

Reviewed by:
Zhentao Yu,
Nanjing University, China
Jinyang Zhang,
Neijiang Normal University, China
Binbin Yu,
Yangzhou University, China
Li-Hua Chen,
Wuhan University of Technology, China

***Correspondence:**
Zhangfa Tong
zhftong@sina.com

Specialty section:
This article was submitted to Colloidal Materials and Interfaces, a section of the journal Frontiers in Materials

Received: *27 November 2018*
Accepted: *10 January 2019*
Published: *04 February 2019*

Citation:
Zhang H, Zhou J, Muhammad Y, Tang R, Liu K, Zhu Y and Tong Z (2019) Citric Acid Modified Bentonite for Congo Red Adsorption. Front. Mater. 6:5. doi: 10.3389/fmats.2019.00005

INTRODUCTION

Dyes are widely used in textile, printing, feather, cosmetics, and plastics industries due to their bright colored and washable nature and sunfast feature (Rosa et al., 2018). However, the effluents discharged by these industries contain untreated dyes which can be toxic to human beings and aquatic life and hence their removal from contaminated wastewater is essential. Various methods such as adsorption over activated carbon (Wen et al., 2016), thermolysis, and coagulation (Yen et al., 2017), membrane separation (Cazzorla et al., 2018; Ye et al., 2018), electrochemical decolorization (Xu L. et al., 2018), photocatalytic degradation (Liu et al., 2019), and biological treatment (Banihani et al., 2018) have been widely reported for the removal of organic pollutants. Among these methods, adsorption over activated carbon is envisaged as highly effective technique. However, the high cost of activated carbon restricts its widespread utilization. On the contrary, low-cost adsorbents including acid treated red mud (Toor et al., 2015), sand (Li P. et al., 2018), raw pine and acid treated pine (Schorr et al., 2018), Ashoka leaf (Shivaprakash et al., 2018), sulphuric acid treated Palm flower (Magdalena et al., 2018), hen feathers (Tesfaye et al., 2018), and clay minerals (Shaban et al., 2018) have been investigated for the treatment of dyes containing wastewater.

Researchers are focusing on the applications of clay minerals attributed to their low-cost, abundant outputs, non-toxicity, stability, and ability of ion exchange. In this regard, several clay minerals such as bentonite (Beheshti et al., 2018; Mat et al., 2018), montmorillonite (Mahmoudian et al., 2018), zeolite (Abdelrahman, 2018), and kaolin (Li Y. et al., 2018) have been reported for the removal of dyes from wastewater. Among these, bentonite had received greater attention as adsorbent due to its high adsorption capacity and cost-effective nature. Mudrinic et al. (2018) studied the removal of acid dyes over sulphuric acid activated bentonite with high adsorption capacity. Baytar et al. (2018) studied removal of methylene blue by acid-activated bentonite and raw bentonite where the former was found more efficient than the later. Ding et al. (2018) reported better efficiency of hydrochloric acid treated bentonite than the nascent version for the removal of Congo Red (CR). Araujo et al. (2018) prepared and effectively applied chitosan and hexadecyl trimethyl ammonium bromide modified bentonite (CTS–CTAB-Bent) absorbent for the removal of weak acid scarlet. These reports suggest that inorganic/organic acid treatment can increase the adsorption capacity of bentonite toward various types of dyes. However, the structure of bentonite could readily be destroyed by strong inorganic acid such as sulphuric acid and hydrochloric acid. Meanwhile, the current commonly used organic modifiers for bentonite includes CTAB, polyacrylic acid, and multi amine-containing gemini surfactants (Li W. Y. et al., 2018; Xu Y. et al., 2018). However, the toxicity and cost of these modifiers and complicated modification technology limit their applications in bentonite modification. Therefore, it is essential to find a suitable, mild, environmentally friendly acid to modify bentonite without compromising on the dye removal efficiency.

As a simple and non-toxic organic acid, citric acid (CA) is very cheap and abundant because it can be obtained from natural biomass. In addition, –OH and –COOH groups in CA are not only effective linking groups for loading CA on RB but also good chelating groups for organic dyes and heavy metals removal. In recent years, some CA-modified adsorbents have been reported for the adsorption of dyes and heavy metals (Wang et al., 2017, 2018; Yan et al., 2018). According to the earlier work in our group, CA can not only modify bentonite environmentally-friendly via a moderate and rapid route but also avoid secondary pollution (Zhou et al., 2015). Thus, CA was selected to modify raw bentonite (RB) to obtain CA modified bentonite (CAB) in this study, which was in turn used for the adsorptive removal of CR. The effect of various factors such as adsorbents dosage, contact time, ionic strength, surfactant, and pH was systematically studied. The adsorption data of CAB and RB were evaluated by kinetic models and isotherm models. To get deeper insight into the adsorption mechanism, RB, and CAB were analyzed by X-rays diffraction (XRD), Brunauer, Emmett, and Teller (BET) surface area analysis and Fourier transform infra-red (FT-IR) spectroscopy.

MATERIALS AND METHODS

Materials

RB was obtained from Shanghai Chemical Co., Ltd, China. CR ([1-napthalene sulfonic acid, 3, 3'-(4, 4'-biphenylenebis (azo)) bis (4-amino-) disodium salt]) was a type of indicator having chemical formula of $C_{33}H_{22}N_6Na_2O_6S_2$, and molecular weight of 696.7 g·mol^{-1}, while its structure is given in **Figure 1**. Cationic CTAB, anionic surfactant sodium dodecyl benzene sulfonate (SDBS), and CA were obtained from Sinopharm Chemical Reagent Co., Ltd, China. All the chemicals were of analytical grade and used without further purification.

Preparation of CAB

CAB was prepared by the following procedure: 5 g of RB was dispersed in 50 mL deionized water in a three-necked flask. 2.78 g CA was dissolved in 50 mL deionized water at room temperature in a separating funnel and the solution was dropwise added into RB dispersion. The mixture was agitated on a magnetic stirrer at 323 K for 3 h, filtered, and washed several times with deionized water and dried at 323 K for 24 h. The adsorbent was ground and sieved through 200 mesh size and kept in a dryer till further analysis/use.

Characterizations of RB and CAB Before and After CR Adsorption

RB, CAB, and CR loaded CAB (CR–CAB) were characterized by XRD (D/MAX 2500 V X-ray diffractometer) with Cu Kα radiation in a 2θ range of 4–60° with a scan speed of 5°/min. The specific surface area and average pore size of RB, ACB, and CR–CAB were determined by a Quantachrome NOVA 1200e volumetric nitrogen adsorption apparatus. The functional groups of samples were studied using FT-IR spectrophotometer (Nicolet FT-IR 6700) in a 4,000–500 cm^{-1} region.

CR Adsorption Studies

Batch adsorption experiments for CR onto RB and CAB were performed. One Hundred milliliter CR solution (200 mg·L^{-1}) with different amounts of adsorbents (0.2–2.0 g·L^{-1}) were taken in conical flasks (250 mL) and agitated using a shaking water bath at 150 rpm at 303 K for fixed time duration. The effect of ionic strength and surfactant on CR adsorption was studied under various concentrations of NaCl, $CaCl_2$, CTAB, and SDBS. The pHs of CR solutions within a range 4–11 were adjusted using 0.1 M NaOH and 0.1 M HCl solutions by a STARTER 3C pH-meter. The kinetic studies of CR adsorption were performed by agitating 100 mL CR solution (100–1,200 mg·L^{-1}) in 250 mL conical flask at 303 K for 12 h until reaching equilibrium. The supernatant of CR was tested for change in concentration at different time intervals. The adsorbent was separated from solution by filtration and filtrate was subjected to centrifugation at 5,000 rpm for 10 min. The supernatants were analyzed by a UV-visible spectrophotometer (UV-2550, Shimadzu) at 498 nm.

CR removal efficiency, the amount of CR adsorbed per unit mass of adsorbent and per unit time were calculated using Equations (1–3), respectively.

$$\eta = \frac{C_0 - C_e}{C_0} \times 100\% \quad (1)$$

$$q_e = \frac{C_0 - C_e}{\frac{m}{V}} \quad (2)$$

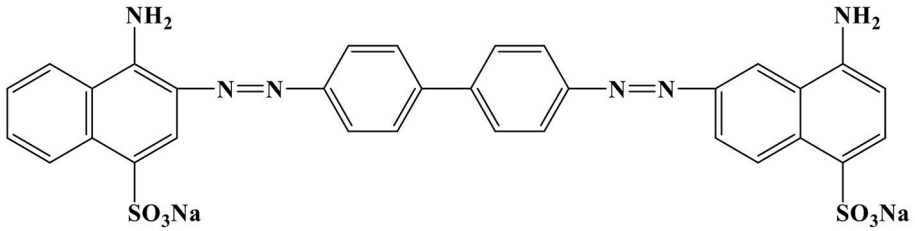

FIGURE 1 | Structure of CR.

$$q_t = \frac{C_0 - C_t}{\frac{m}{V}} \quad (3)$$

where η is the removal efficiency of the adsorbent, q_e, and q_t are the adsorption capacity ($mg{\cdot}g^{-1}$), at equilibrium time and at any given time, respectively. C_0, C_e, and C_t are the concentrations ($mg{\cdot}L^{-1}$), of the dye at initial time, at equilibrium time, and at any given time, respectively. m is the mass (g) of adsorbent and V is the volume (mL) of dye solution.

Adsorption Isotherm Studies

Adsorption isotherm models such as Langmuir (Sha et al., 2018) and Freundlich (Xavier et al., 2018) are commonly used for the fitting of experimental data. Parameters of each model can explain the adsorption mechanisms between the adsorbate and adsorbent. The linear forms of Langmuir and Freundlich models are presented in Equations (4, 5), respectively:

$$\frac{C_e}{q_e} = \frac{1}{q_{\max} K_L} + \frac{C_e}{q_{\max}} \quad (4)$$

$$\ln q_e = \ln K_F + \frac{1}{n} \ln C_e \quad (5)$$

where $q_{\max}$ is the theoretical estimation of maximum adsorption capacity, K_L ($L{\cdot}mg^{-1}$) is the Langmuir isotherm constant related to the energy of adsorbate/adsorbent interaction. K_F ($mg{\cdot}g^{-1}$) and n are the Freundlich constants related to adsorption capacity and adsorption intensity, respectively.

The kinetic models are equations which reflect the relationship of adsorption time and adsorption capacity. Thus, kinetic data from CR adsorption on RB and CAB was evaluated by pseudo-first kinetic model (Bernstein et al., 2018), pseudo-second kinetic model (Bernstein et al., 2018), and intra-particle diffusion model (Olivoalanis et al., 2018) using their linear forms shown by Equations (7–9), respectively.

$$\log(q_e - q_t) = \log q_e - \frac{k_1}{2.303} t \quad (6)$$

$$\frac{t}{q_t} = \frac{1}{k_2 q_e^2} + \frac{1}{q_e} t \quad (7)$$

$$q_t = k_{id} t^{1/2} + I \quad (8)$$

where k_1 (min^{-1}) and k_2 ($g{\cdot}mg^{-1}{\cdot}min^{-1}$) are the rate constants of pseudo-first kinetic model and pseudo-second kinetic model, respectively, at time t (min). k_{id} ($mg{\cdot}g^{-1}{\cdot}min^{-1/2}$) and I ($mg{\cdot}g^{-1}$) are the intra-particle model constants.

RESULTS AND DISCUSSION

Effect of Various Experimental Conditions on CR Adsorption

Effect of Adsorbent Dosage on CR Adsorption

The effect of various dosages of RB and CAB on the removal of CR was tested and the results are compiled in **Figure 2**. The removal of CR increased sharply with increasing dosage of CAB from 0.2 to 1 $g{\cdot}L^{-1}$ and then reached to equilibrium. While for RB, the removal of CR increased gradually over the dosage range, which indicated direct relation between amount of adsorbent and active sites (Fosso et al., 2016). The active adsorption sites increased with increasing adsorbent dosage, which ultimately led to grater CR adsorption. CR removal by RB and CAB increased from 13 to 74% and 30 to 92%, respectively, by increasing adsorbent dosage from 0.2 to 2.0 $g{\cdot}L^{-1}$. However, CR adsorption capacity decreased with increasing adsorbent dosage, which could be attributed to aggregation of adsorption sites with each other resulting in decreasing total surface area available to CR and increase in diffusion path length (Bernstein et al., 2018). In **Figure 2**, the optimum dosage of CAB was 1 $g{\cdot}L^{-1}$ was chosen for onward experiments.

Effect of Contact Time on CR Adsorption

The results for the effect of contact time on CR adsorption by CAB and RB are plotted in **Figure 3**, which suggests that the removal efficiency of CR on both adsorbents increased with increasing contact time from 0 to 90 min and attained equilibrium afterwards. **Figure 3** further suggests that CR removal on RB was only 20% within 5 min which slowly reached to 54% after 450 min. Compared with RB, CAB showed better adsorption capacity for CR i.e., CR removal efficiency by CAB in first 5 min was 45%, which was enhanced to 87% after 120 min. By comparing the CR removal efficiency (87%) by CAB with some literature reports, one can conclude that the newly designed CAB had faster reaction kinetics and hence can be deemed greatly cost effective on industrial level applications (Toor et al., 2015; Tarmizi et al., 2017).

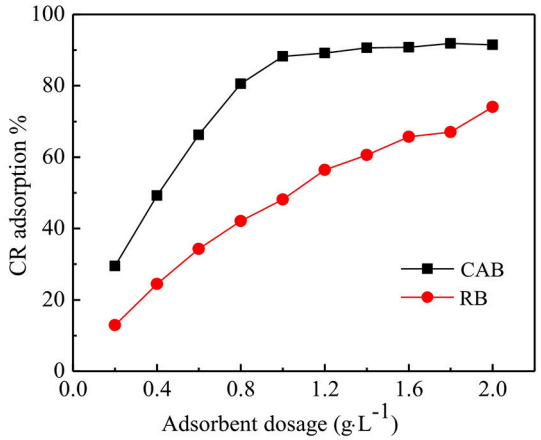

FIGURE 2 | Effect of adsorbent dosage on CR adsorption on RB and CAB.

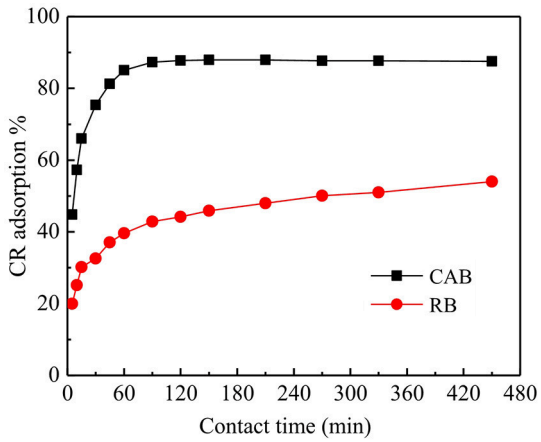

FIGURE 3 | Effect of contact time on CR adsorption on RB and CAB.

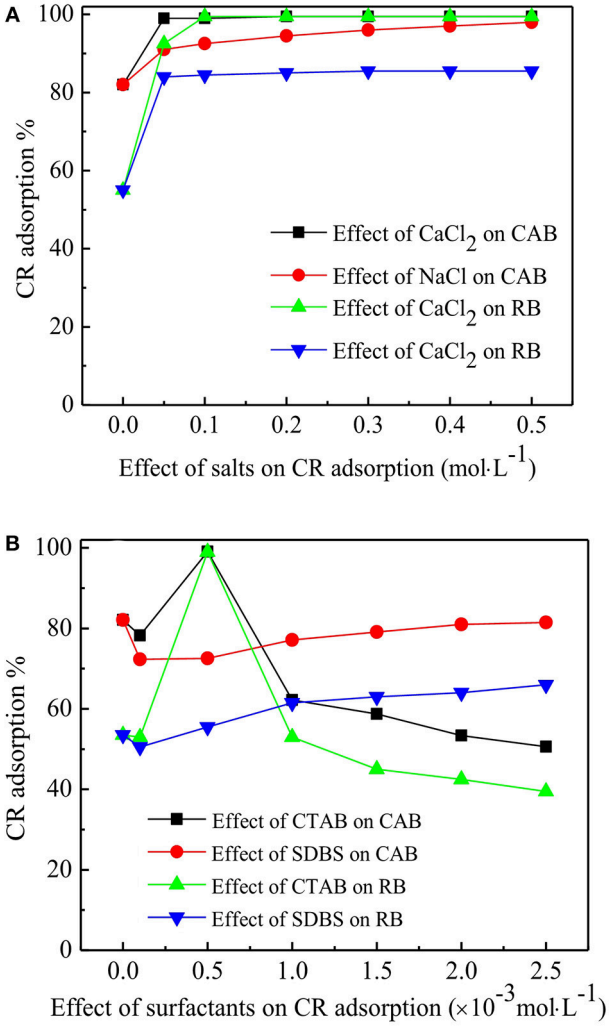

FIGURE 4 | Effect of inorganic salt **(A)** and surfactants **(B)** on CR adsorption on RB and CAB.

Effect of Ionic Strength and Surfactant on CR Adsorption

The effect of NaCl and $CaCl_2$ concentration (0–0.5 mol·L^{-1}) on CR adsorption were studied and the results are compiled in **Figure 4A**. An increase in CR removal was observed by increasing slat concentration of NaCl and $CaCl_2$ from 0 to 0.05 M and became constant onward. The increase in CR removal with increasing salts' concentration could be credited to decrease in the electrostatic repulsion between CR anions, thus accelerating CR aggregation (Lin et al., 2018). In addition, compared with NaCl, higher enhancement in CR removal was observed by the presence of $CaCl_2$, which could be due to the presence of more positive charge on Ca^{2+} than Na^{+}, hence bitterly neutralizing negative charges in aqueous solution. Furthermore, Ca-dye precipitation could occur in CR solution with the existence of Ca^{2+} (Hadjltaief et al., 2018), while the aggregation of CR and Ca-CR precipitation could also be counted toward better CR removal.

Surfactants are widely used in the treatment of dyes, thus the effect of cationic surfactant (CTAB) and anionic surfactant (SDBS) in a concentration range of 0.1 and 2.5 mM, were investigated on CR adsorption. The results compiled in **Figure 4B** suggest that in the presence of 0.5 mM CTAB, a CR removal of up to 99% was achieved on RB and CAB. However, further increase in CTAB concentration led to decrease in CR removal. This could be accredited to the fact that at low CTAB concentration, surfactant monomers firstly adsorbed to adsorbent surface, creating additional positive charges which electrostatically increased CR adsorption (Sham and Notley, 2018). Decrease in CR removal efficiency above critical micelle concentration (CMC) of CTAB was due to micelle formation and dye solubilization (Gorsd et al., 2018; Sham and Notley, 2018). The micelles were formed at high CTAB concentration which solubilized CR molecules, hence preventing CR adsorption. However, researchers (Yao et al., 2012; Gorsd et al., 2018) have

reported far lower residual concentration of CTAB than its CMC when the dye removal efficiency started to decline, which could be attributed to the pore-blocking on the adsorbent surface. **Figure 4B** shows that at a low concentration of SDBS, CR removal decreased slightly, and then ascended gradually on both CAB and RB. Anionic surfactants have been reported to have different influence on different anionic dyes and hence their chemical structures play an important role on dye adsorption (Lee et al., 2018; Zhou et al., 2018).

Effect of pH on CR Adsorption

Figure 5 shows that pH exhibited different effect on CR removal by CAB and RB. CR removal by RB decreased from 76 to 49% with increasing pH, which could be due to the dissociation of sulfonate groups of CR (D-SO_3Na) in aqueous medium producing anionic dye ions (Jia et al., 2018). At low pH, the negative surface of RB was efficiently neutralized by H^+ ions thereby reducing hindrance for the spreading of CR. In addition, electrostatic attraction between RB and the anionic dye ions promote CR adsorption in acidic condition. As pH increased, the number of negatively charged sites on RB increased enhancing the electrostatic repulsion hence hindering CR adsorption. Moreover, the competitions for adsorption active sites occurred between OH^- and anionic dye ions with increasing pH. CR removal by CAB increased with increasing pH from 4 to 6 followed by a decline with further increase in pH. The highest CR removal by RB and CAB was above 83%, which was achieved at neutral and weak acidic pH. The plots of absorbance vs. wavelength for CR adsorption on CAB at various pH (4–11) (**Figure 6**) suggested that the maximum adsorption wavelength of CR (498 nm) barely altered with pH. Hence, CR remained stable within pH 4–11 range and thus CAB removed CR mainly by adsorption.

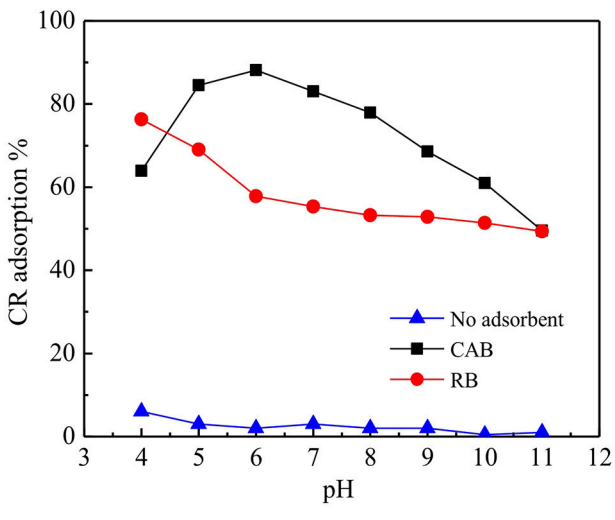

FIGURE 5 | Effect of pH on CR adsorption on RB and CAB.

Adsorption Isotherms

The Langmuir adsorption isotherm is applied for calculating monolayer adsorption with the basic assumption that sorption takes place at specific homogeneous sites within the adsorbent (Xavier et al., 2018). The maximum adsorption capacity (q_m) represents the saturated monolayer adsorption at equilibrium. The Freundlich equation is an empirical equation for describing adsorbate on the heterogeneous surface of the adsorbent. The affinity between the adsorbate and the adsorbent could be indicated by heterogeneous factor, $1/n$. The isotherm parameters are presented in **Table 1**. The saturated adsorption capacities at 303 K for CAB and RB were 384 and 250 $mg{\cdot}g^{-1}$, respectively. The Freundlich parameter, $0 < 1/n < 1$, indicated favorable of CR adsorption on CAB and RB. The correlation coefficient R^2 of Langmuir was 0.99, much higher than that of Freundlich isotherm, indicating better fit of experimental data with the Langmuir model. The preparation conditions and CR adsorption performance of various adsorbents were compared with the present work in **Table 2** (Zhang et al., 2013; Srivastava and Sillanpää, 2016; Huang et al., 2017; Said et al., 2017; Shaba et al., 2017; Shaban et al., 2018). Compared with the traditional methods of clay adsorbents synthesis, present work can considerably shorten the reaction time. Moreover, CAB was prepared under a more moderate pH range using a non-toxic, abundant low-molecular organic acid (CA), which can reduce the adsorbent cost, and avoid secondary pollution. Therefore, this synthesis method of

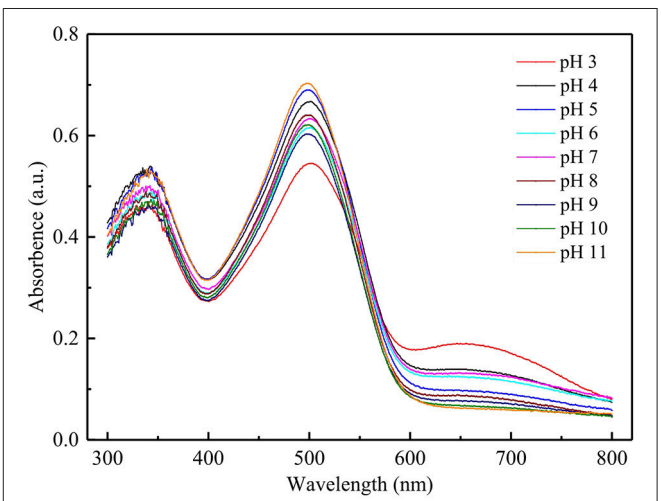

FIGURE 6 | The UV-vis absorbance spectra of CR within experimental pH range.

TABLE 1 | Parameters of isotherm models for CR adsorption on RB and CAB (q_{max}: $mg{\cdot}g^{-1}$, k_L: $L{\cdot}mg^{-1}$, k_f: $mg{\cdot}g^{-1}$).

Adsorbent	Langmuir model			Freundlich model		
	q_m	$K_L \times 10^{-2}$	R^2	K_F	$1/n$	R^2
RB	250	0.71	0.996	19.9	0.362	0.981
CAB	384	255	0.999	59.6	0.294	0.901

CAB was competitive with reported ones. It also noted that CAB removal efficiency was comparable to other adsorbents for CR removal from aqueous solution at lower adsorbent dosage and short equilibrium time. The Langmuir adsorption capacity of CAB for CR was 1.6–19.2 times higher than that of reported literature (malachite@bentonite and bentonite with organometallic $[Fe_3O(OOC_6H_5)_6(H_2O)_3(NO_3).nH_2O]$, respectively) (Srivastava and Sillanpää, 2016; Said et al., 2017). Keeping in mind the enhanced adsorption performance with simple preparation technology and cost effectiveness, CAB could be deemed a promising adsorbent for dyes removal from wastewater.

Adsorption Kinetics

Pseudo-first-order, pseudo-second-order, and intra-particle diffusion models were applied to analyze the kinetics of CR adsorption. The parameters of kinetic models were calculated from the best fitting plots listed in **Table 3**, which suggest that

TABLE 2 | Comparison of preparation conditions and adsorption performance of various adsorbents for CR removal.

Adsorbent	Preparation conditions	Adsorption conditions	Langmuir capacities ($mg \cdot g^{-1}$)	References
Alkaline Ca- bentonite	Modifier: CaO Temperature: 60°C Reaction time: 3 h pH: 10	Dosage: 2.0 $g \cdot L^{-1}$ CR: 100 $mg \cdot L^{-1}$ Time: 2 h pH: 7	149	Zhang et al., 2013
Insertion of bentonite with organometallic $[Fe_3O(OOC_6H_5)_6(H_2O)_3(NO_3).nH_2O]$	Modifier: $[Fe_3O(OOC_6H_5)_6(H_2O)_3(NO_3).nH_2O]$ Room temperature Reaction time: 24 h pH: 10 N_2 protection	Dosage: 0.6 $g \cdot L^{-1}$ CR: 150 $mg \cdot L^{-1}$ Time: 1 h pH: 7	20	Said et al., 2017
CTAB/bentonite	Modifier: CTAB Temperature: 60°C Reaction time: 7 h pH: 7	Dosage: 2.0 $g \cdot L^{-1}$ CR: 300 $mg \cdot L^{-1}$ Time: 1.5 h pH: 8	157	Huang et al., 2017
Malachite@clay	NO modifier Room temperature Reaction time: 2 h pH: 7	Dosage: 2.0 $g \cdot L^{-1}$ CR: 300 $mg \cdot L^{-1}$ Time: 3 h pH: 7	238	Srivastava and Sillanpää, 2016
Bentonite/Zeolite-NaP	NO modifier Temperature: 150°C Reaction time: 6 h pH: 12	Dosage: 0.2 $g \cdot L^{-1}$ CR: 10 $mg \cdot L^{-1}$ Time: 4 h pH: 5	46	Shaban et al., 2018
Inorganic- and organic-modified kaolinite	Modifier: $CTAB/CH_3COONa/Na_3PO_4/Na_2SO_4$ Temperature: 50°C Reaction time: 24 h Non-buffered pH	Dosage: 0.7 $g \cdot L^{-1}$ CR: 100 $mg \cdot L^{-1}$ Time: 2 h pH: 7	149	Shaba et al., 2017
RB	NO modifier Temperature: 60°C Reaction time: 3 h pH: 7	Dosage: 1.0 $g \cdot L^{-1}$ CR: 200 $mg \cdot L^{-1}$ Time: 1.5 h pH: 7	250	Present study
CAB	Modifier: citric acid Temperature: 60°C Reaction time: 3 h pH: 7	Dosage: 1.0 $g \cdot L^{-1}$ CR: 200 $mg \cdot L^{-1}$ Time 1.5 h pH: 6	384	Present study

TABLE 3 | Parameters of kinetic models for CR adsorption on RB and CAB.

Adsorbent	$q_{e,exp}$	Pseudo-first-order model			Pseudo-second-order model			Intra-particle diffusion model		
		$q_{e,cal}$	$k_1 \times 10^{-3}$	R^2	$q_{e,cal}$	$k_2 \times 10^{-4}$	R^2	k_{i2}	I	R^2
RB	107	64.4	9.60	0.901	108	4.64	0.997	1.90	68.1	0.995
CAB	175	14.9	11.2	0.484	178	15.4	1.000	9.90	95.0	0.991

the R^2 of pseudo-second-order kinetic model were higher than the other two models. The calculated q_e values were consistent with the experimental ones, which concluded the better fit of CR adsorption data on RB and CAB to pseudo-second kinetic model.

Normally, the intra-particle diffusion model could be divided into three parts. The first part showed the diffusion of adsorbate to external surface of the adsorbent or boundary layer diffusion. The second part describes the gradual adsorption stage where the intra-particle diffusion rate is considered as the rate-limiting factor, while the last part is the equilibrium stage (Bernstein et al., 2018; Olivoalanis et al., 2018). The fitting plots of q_t vs. $t^{0.5}$ are shown in **Figure 7**. The fitting plots for CR adsorption by CAB could be divided into three parts, hence, three steps involved in the adsorption process, i.e., CR molecules diffused rapidly on the surface of CAB, then penetrated into the interior surface of CAB and reached adsorption equilibrium at last. The adsorption process could be divided into two steps on RB i.e., one for the boundary layer diffusion and the other for the intra-particle diffusion. The plots do not pass through the origin indicating that intra-particle diffusion was involved in the adsorption process, though it was not the only rate-limiting step.

Characterizations of Nascent and CR Loaded Adsorbents

X-ray Diffraction and Pore Structures

Table 4 presents the parameters of basal spacing and pore structures of various samples. Compared with the RB, the specific area of CAB decreased which could be attributed to CA activation resulting in decrease in micro-pores and increase in the number of meso-pores. The pore diameter of CAB was larger than that of RB, which corresponded with the higher reaction rate shown in **Table 3** (Tohdee et al., 2018). The decrease in BET surface area of CR-CAB may be caused by two mechanisms: (1) CR ions may screen CAB surface, which was inaccessible by the nitrogen molecules; (2) CR molecules may have blocked some smaller pores and inhibit the passage of nitrogen molecules into these pores (Mahmoudian et al., 2018). **Table 4** also showed the value of basal spacing of RB, CAB, and CR-CAB. The 2θ of RB at 5.7 was the characteristic basal spacing (d_{001}) of 1.55 nm for calcium bentonite (Zhang et al., 2011). After CA modification, the basal spacing of CAB changed compared with RB. The d_{001} spacing of CR-CAB increased only 0.03 nm which implied CR molecule did not penetrate into CAB interlayer space, i.e., CR adsorption by CAB was mainly controlled by surface adsorption since the molecule dimensions of CR are 3.00 nm wide, 0.73 nm deep, and 0.25 nm thick (Mi et al., 2017).

FT-IR

FT-IR spectra of CAB and RB before and after CR adsorption are shown in **Figure 8**. For RB and CAB, the bands at 1,036 and 524 cm^{-1} were due to Si-O-Si and Si-O-Al (where Al comes from an octahedral cation) stretching peaks, respectively (Brito et al., 2018). The bands at 3,613 and 3,419 cm^{-1} corresponding to –OH stretching vibration of adsorbed water and hydrogen bonding between water molecules and Si-O surface, respectively (Zhang et al., 2014). The new adsorption band in CAB at 1,732 cm^{-1} was assigned to C=O symmetrical stretching, which obviously related to carboxyl groups of CA (Sonia et al., 2018). The main binding modes of CA on bentonite are as follows: (1) Esterification reaction between bentonite and CA. Abundant -OH groups on the surface of RB can react with CA by forming an ester linkage and thus introduce carboxyl groups in CAB

TABLE 4 | Basal spacing, BET surface area, total pore volume, and pore diameter of RB, CAB, and CR-CAB.

Adsorbent	D-spacing (nm)	BET surface area ($m^2 \cdot g^{-1}$)	Total pore volume ($cm^3 \cdot g^{-1}$)	Pore diameter (nm)
RB	1.55	40.1	0.07	8.06
CAB	1.54	16.4	0.06	11.7
CR-CAB	1.57	11.5	0.05	15.5

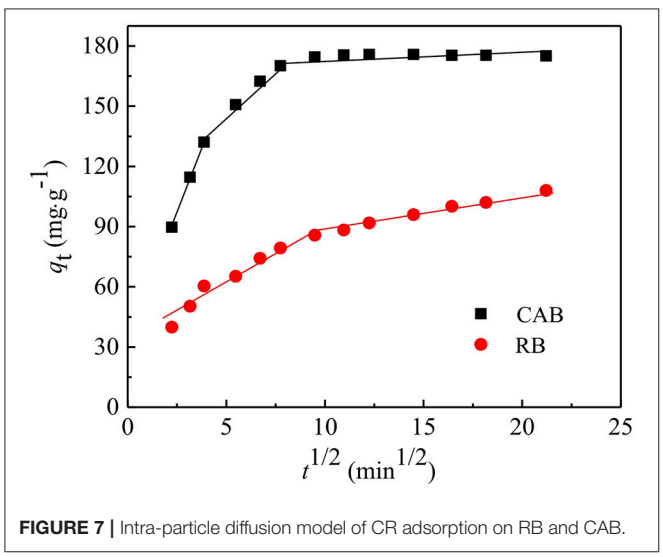

FIGURE 7 | Intra-particle diffusion model of CR adsorption on RB and CAB.

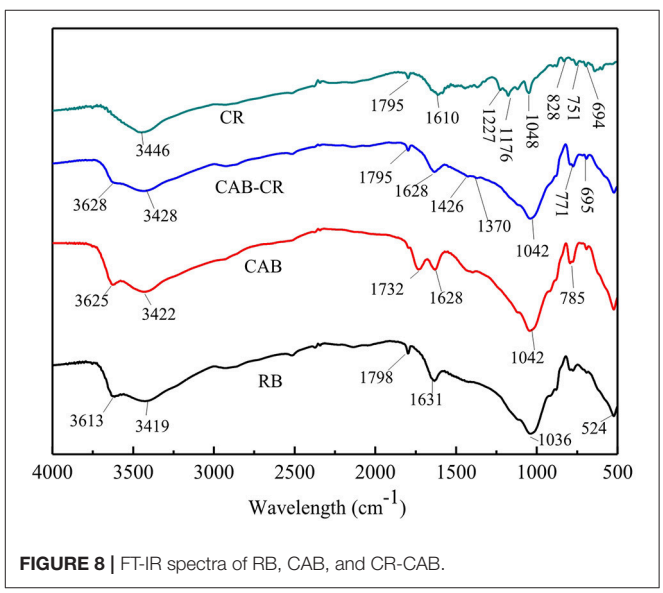

FIGURE 8 | FT-IR spectra of RB, CAB, and CR-CAB.

(**Figure 9**) (El-Sheikh et al., 2018; Liu et al., 2018). (2) Cation exchange reaction between hydrogen ions from CA and the exchange cations (such as Na, Ca, and Mg) in RB interlayer via the following reaction.

$$CA^{n-}—nH^{+} + M^{n+}—\text{Bentonite} \rightarrow M^{n+} + CA—\text{Bentonite} \quad (9)$$

where M and *n* are the exchangeable cation in RB interlayer and the corresponding valence of the cation, respectively. By the cation exchange reaction, CA can bond with RB easily (Bulut et al., 2008; Gong et al., 2018).

The band diminished after CR adsorption and new bands at 1,426 and 1,370 cm^{-1}, which corresponded to symmetric vibration and asymmetric vibration of -COO^{-}, respectively (Rossi et al., 2018). –COOH of CA ionized to give H^{+} and -COO^{-}, and CR ions were protonated by H^{+} ions when CR molecules reached the edge of CAB. Therefore, there existed an electrostatic interaction between the protonated CR ions and negatively charged groups of CAB. The band at 3,446 cm^{-1} corresponded to –N-H- stretching vibration and 1,610 cm^{-1} was assigned to -N=N- stretching in the structure of CR, which diminished after CAB adsorption, while the peaks at 1,176 and 1,048 cm^{-1} assigned to S=O stretching (Sonia et al., 2018) also diminished. Hence, chances of hydrogen bonding or esterification may exist between the functional electronegative groups on CR such as -NH_2, -N=N-, -SO_3, -OH, and -COOH groups of CAB. Therefore, CR adsorption by CAB was a chemical adsorption process and the main active adsorption sites were -NH_2, -N=N-, -SO_3, -OH, and -COOH groups.

Adsorption Mechanism of CR on ACB

The main adsorption mechanism of CAB for CR removal included chelation, hydrogen bonding, and fixation. (1) Good chelating ability toward CR. The -COOH groups of citric acid were not only used as linking groups for coating CA on RB, but also provided active adsorption sites for CR via chelation (**Figure 10**) (Yin et al., 2018). The chelation between –COOH on CAB and -NH_2 on CR has also been confirmed by the FT-IR results analysis. (2) Hydrogen bonding. Abundant -OH groups on CAB can bind with more electronegative groups including -NH_2, -N=N- or -SO_3 on CR and thus form hydrogen bonds (Feng et al., 2017). It is also crucial for CR adsorption on CAB. (3) Fixation is also a principal mechanism for dyes removal by the clay materials. CAB has a number of micropores and mesopores, so CR may diffuse and be fixed into the pore spaces of CAB structure (Zhao et al., 2018). Adsorption kinetics fitting results especially intraparticle diffusion model has confirmed that CR adsorption on CAB involves pore-filling by diffusing. In addition, BET surface area of CAB before and after CR adsorption also indicated that a certain amount of CR was fixed on CAB by physical adsorption.

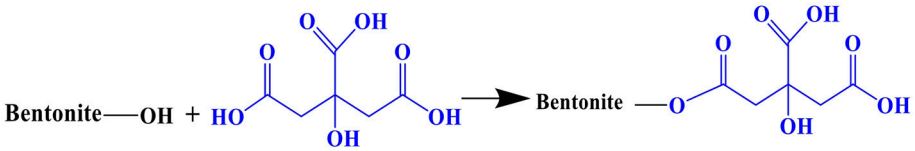

FIGURE 9 | Esterification reaction of bentonite and critic acid.

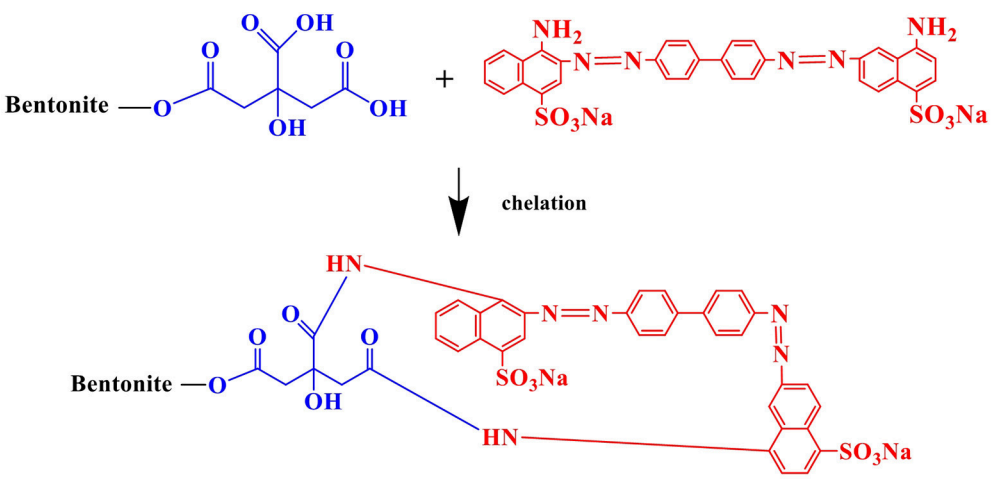

FIGURE 10 | Chelation between CAB and CR.

CONCLUSIONS

In this study, CAB was prepared by modifying RB with CA and its adsorption performance for CR was investigated. Experimental results showed that adsorption capacity of CR on CAB was higher (384 $mg \cdot g^{-1}$) with much faster kinetics than that on RB. In addition, adsorption of CR on RB and CAB was seriously influenced by pH, concentration of NaCl, $CaCl_2$, and CTAB. The isotherm studies revealed that Langmuir model could better describe CR adsorption, while kinetic data best fitted with pseudo-second order model. CR adsorption on CAB was a chemical process including chelation, hydrogen bonding, and fixation, which controlled by the active adsorption sites (–OH and –COOH) of CAB surface. This study credited to the ease and facile synthesis approach for CAB with high adsorption efficiency for CR, can be deemed as a promising approach for industrial waste-water treatments.

AUTHOR CONTRIBUTIONS

HZ conceived and designed the experiments. JZ, RT, and KL contributed through execution and optimization of experiments along with analysis of data. ZT contributed reagents, materials, analysis tools. YM and YZ wrote the paper. All authors have read and approved the final manuscript.

ACKNOWLEDGMENTS

We acknowledge the National Nature Science Foundation of China (Grant No. 21166004 and 21576055) for the financial support.

REFERENCES

Abdelrahman, E. A. (2018). Synthesis of zeolite nanostructures from waste aluminum cans for efficient removal of malachite green dye from aqueous media. *J. Mol. Liq*. 253, 72–82. doi: 10.1016/j.molliq.2018.01.038

Banihani, A., Deery, C., Toumba, J., and Duggal, M. (2018). Effectiveness, costs and patient acceptance of a conventional and a biological treatment approach for carious primary teeth in children. *Caries Res*. 53, 65–75. doi: 10.1159/000487201

Baytar, O., Sahin, O., Saka, C., and Agrak, S. (2018). Characterization of microwave and conventional heating on the pyrolysis of pistachio shells for the adsorption of methylene blue and iodine. *Anal. Lett*. 51, 2205–2220. doi: 10.1080/00032719.2017.1415920

Beheshti, A., Nozarian, K., Ghamari, N., Mayer, P., and Motamedi, H. (2018). Selective high capacity adsorption of Congo Red, luminescence and antibacterial assessment of two new Cadmium(II) coordination polymers. *J. Solid State Chem. France* 258, 618–627. doi: 10.1016/j.jssc.2017.11.035

Bernstein, O. M., Mcgee, T. E., Silzel, L. E., and Silzel, J. W. (2018). Fluorescent pseudorotaxanes of a quinodicarbocyanine dye with gamma cyclodextrin. *Spectrochim Acta A* 189, 202–214. doi: 10.1016/j.saa.2017.07.060

Brito, D. F., Edson, C., Fonseca, G., and Maria, G. (2018). Organophilic bentonites obtained by microwave heating as adsorbents for anionic dyes. *J. Environ. Chem. Engin*. 6, 7080–7090. doi: 10.1016/j.jece.2018.11.006

Bulut, E., Ozacar, M., and Sengil, I. A. (2008). Equilibrium and kinetic data and process design for adsorption of Congo Red onto bentonite. *J. Hazard Mater*. 154, 613–622. doi: 10.1016/j.jhazmat.2007.10.071

Cazzorla, C., Bensi, G., Biasucci, G., Leuzzi, V., Manti, F., Musumeci, A., et al. (2018). Living with phenylketonuria in adulthood: the pku attitude study. *Mol. Genet. Meta*. 16, 39–45. doi: 10.1016/j.ymgmr.2018.06.007

de Araújo M. J. G., Barbosa, R. C., Fook, M., Canedo, E. L., Silva, S., and Medeiros, E. S. (2018). HDPE/Chitosan Blends modified with organobentonite synthesized with quaternary ammonium salt impregnated chitosan. *Materials* 11:291. doi: 10.3390/ma11020291

Ding, S., Sun, Q., Chen, X., Liu, Q., Wang, D., and Lin, J. (2018). Synergistic adsorption of phosphorus by iron in lanthanum modified bentonite (phoslock): new insight into sediment phosphorus immobilization. *Water Res*. 134, 32–43. doi: 10.1016/j.watres.2018.01.055

El-Sheikh, A. H., Fasfous, I. I., Al-Salamin, R. M., and Newman, A. P. (2018). Immobilization of citric acid and magnetite on sawdust for competitive adsorption and extraction of metal ions from environmental waters. *Chem. Eng. J*. 4, 5186–5195. doi: 10.1016/j.jece.2018.08.020

Feng, Y., Liu, Y., Xue, L., Sun, H., Guo, Z., Zhang, Y., et al. (2017). Carboxylic acid functionalized sesame straw: a sustainable cost-effective bioadsorbent with superior dye adsorption capacity. *Bioresource Technol*. 238, 675–683. doi: 10.1016/j.biortech.2017.04.066

Fosso, K., Frans, W., and Fourie, C. L. (2016). Adsorption of Congo Red by surfactant-impregnated bentonite clay. *Desalin Water Treat*. 57, 27663–27671. doi: 10.1080/19443994.2016.1177599

Gong, N., Liu, Y. P., and Huang, R. H. (2018). Simultaneous adsorption of Cu2+ and Acid fuchsin (AF) from aqueous solutions by CMC/bentonite composite. *Int. J. Biol. Macromol*. 115, 580–589. doi: 10.1016/j.ijbiomac.2018.04.075

Gorsd, M. N., Sosa, A. A., Frenzel, R. A., and Pizzio, L. R. (2018). Synthesis and characterization of tungstophosphoric acid-modified mesoporous sponge-like tud-1 materials. *J. Sol. Gel. Sci. Techn*. 87, 204–215. doi: 10.1007/s10971-018-4677-z

Hadjltaief, H. B., Ameur, S. B., Costa, P. D., Zina, M. B., and Galvez, M. E. (2018). Photocatalytic decolorization of cationic and anionic dyes over ZnO nanoparticle immobilized on natural tunisian clay. *Appl. Clay Sci*. 152, 148–157. doi: 10.1016/j.clay.2017.11.008

Huang, Z. H., Li, Y. Z., Chen, W. J., Shi, J. H., and Zhang, Y. X. (2017). Modified bentonite adsorption of organic pollutants of dye wastewater. *Mater. Chem. Phys*. 202, 266–276. doi: 10.1016/j.matchemphys.2017.09.028

Jia, X. J., Wang, J., Wu, J., Teng, W., Zhao, B., and Li, H. (2018). Facile synthesis of $MoO_2/CaSO_4$ composites as highly efficient adsorbents for Congo Red and Rhodamine B. *Rsc Adv*. 8, 1621–1631. doi: 10.1039/C7RA11292K

Lee, W., Yoon, S., Choe, J. K., Lee, M., and Choi, Y. (2018). Anionic surfactant modification of activated carbon for enhancing adsorption of ammonium ion from aqueous solution. *Sci. Total Environ*. 639, 1432–1439. doi: 10.1016/j.scitotenv.2018.05.250

Li, P., Gao, B., Li, A., Hu, L., and Yang, H. (2018). Highly selective adsorption of dyes and arsenate from their aqueous mixtures using a silica-sand/cationized-starch composite. *Micropor. Mesopor. Mat*. 263, 210–219. doi: 10.1016/j.micromeso.2017.12.025

Li, W. Y., Bai, Y. S., Ma, Q. L., Chen, W. J., Wu, M., and Ma, H. Z. (2018). Polyacrylic acid/ctab-bentonite coated filter paper: efficient and rapid removal of anionic and cationic dyes. *Appl. Surf. Sci*. 458, 903–909. doi: 10.1016/j.apsusc.2018.07.169

Li, Y., Meas, A., Shan, S., Yang, R., Gai, X., and Wang, H. (2018). Characterization, isotherm and kinetic data for adsorption of Congo Red and 2-naphthol on different bamboo hydrochars. *Data Brief*. 19, 49–54. doi: 10.1016/j.dib.2018.04.066

Lin, J., Jiang, B., and Zhan, Y. (2018). Effect of pre-treatment of bentonite with sodium and calcium ions on phosphate adsorption onto zirconium-modified bentonite. *J. Environ. Manage*. 217, 183–195. doi: 10.1016/j.jenvman.2018.03.079

Liu, K., Qin, Y. L., Muhammad, Y., Zhu, Y., Tang, R., and Zhang, H. B. (2019). Effect of Fe_3O_4 content and microwave reaction time on the properties of Fe_3O_4/ZnO magnetic nanoparticles. *J. Alloy Compd*. 781, 790–799. doi: 10.1016/j.jallcom.2018.12.085

Liu, X., Xu, L., Liu, Y., and Zhou, W. (2018). Synthesis of citric acid-modified resins and their adsorption properties towards metal ions. *R. Soc. Open Sci.* 8, 167–177. doi: 10.1098/rsos.171667

Magdalena, R., Hassanein, M. M. M., Abdel-Razek, A. G., Kmiecik, D., Siger, A., and Ratusz, K. (2018). Influence of composition on degradation during repeated deep-fat frying of binary and ternary blends of palm, sunflower and soybean oils with health-optimised saturated-to-unsaturated fatty acid ratios. *Int. J. Food Sci. Tech.* 53, 1021–1029. doi: 10.1111/ijfs.13678

Mahmoudian, M., Balkanloo, P. G., and Nozad, E. (2018). A facile method for dye and heavy metal elimination by pH sensitive acid activated montmorillonite/polyethersulfone nanocomposite membrane. *Chin. J. Polym. Sci.* 36, 49–57. doi: 10.1007/s10118-018-2004-3

Mat, S. S. A., Zuber, S. Z. H. S., Rahim, S. K. E. A., Sohaimi, K. S. A., Halim, N. A. A., and Zainudin, N. F. (2018). Malachite green adsorption by spent coffee grounds. *Mater. Sci. Eng.* 318, 12–15.doi: 10.1088/1757-899X/318/1/012015

Mi, J., Gregorich, E. G., Xu, S., Mclaughlin, N. B., Ma, B., and Liu, J. (2017). Effect of bentonite amendment on soil hydraulic parameters and millet crop performance in a semi-arid region. *Field Crop Res.* 212, 107–114. doi: 10.1016/j.fcr.2017.07.009

Mudrinic, T. M., Ajdukovic, M. J., Jovic-Jovicic, N. P., Marinovic S. R., Mojovic, Z. D., Milutinović-Nikolić, A. D., et al. (2018). Al, Fe, Ni-pillared bentonite in the catalytic wet peroxide oxidation of the textile dye acid yellow 99. *React. Kinet. Mech. Cat.* 124, 75–88. doi: 10.1007/s11144-018-1386-0

Olivoalanis, D., Garciareyes, R. B., Alvarez, L. H., and Garciagonzalez, A. (2018). Mechanism of anaerobic bio-reduction of azo dye assisted with lawsone-immobilized activated carbon. *J. Hazard Mater.* 347, 423–430. doi: 10.1016/j.jhazmat.2018.01.019

Rosa, A. D., Elvis, C., Guilherme, L. D., Hedda, S., and Liliana, A. F. (2018). Biosorption of rhodamine B dye from dyeing stones effluents using the green microalgae *Chlorella pyrenoidosa*. *J. Clean. Prod.* 198, 1302–1310. doi: 10.1016/j.jclepro.2018.07.128

Rossi, T. J., Escobedo, J., Santos, C. M. D., Rossi, L. R., Silva, B. P. D., and Pai, E. D. (2018). Global, diffuse and direct solar radiation of the infrared spectrum in botucatu/sp/ brazil. *Renew. Sust. Energy Rev.* 82, 448–459. doi: 10.1016/j.rser.2017.09.030

Said, M., Utami, H. P., and Hayati, F. (2017). Insertion of bentonite with organometallic $[Fe_3O(OOC_6H_5)6(H_2O)_3(NO_3).nH_2O]$ as adsorbent of Congo Red. *IC2MS* 299:012086. doi: 10.1088/1757-899X/299/1/012086

Schorr, D., Blanchet, P., and Essoua, G. G. E. (2018). Glycerol and citric acid treatment of lodgepole pine. *J. Wood Chem. Technol.* 2, 123–136. doi: 10.1080/02773813.2017.1388822

Sha, Z., Luo, X., Liao, X., Wang, S., Wang, Q., and Chen, S. (2018). Preparation and characterization of the inclusion complex of astaxanthin. *J. Korean Phys. Soc.* 72, 1228–1236.

Shaba, M., Sayed, M. I., Mohamed, G., and Zeinab, M. (2017). Adsorption behavior of inorganic- and organic-modified kaolinite for Congo red dye from water, kinetic modeling, and equilibrium studies. *J. Sol-Gel. Sci. Tech.* 81, 421–447. doi: 10.1007/s10971-018-4719-6

Shaban, M., Abukhadra, M. R., Shahien, M. G., and Ibrahim, S. S. (2018). Novel bentonite/zeolite-nap composite efficiently removes methylene blue and Congo Red dyes. *Environ. Chem. Lett.* 2, 275–280. doi: 10.1007/s10311-017-0658-7

Sham, A. Y. W., and Notley, S. M. (2018). Adsorption of organic dyes from aqueous solutions using surfactant exfoliated graphene. *J. Environ. Chem. Eng.* 6, 495–504. doi: 10.1016/j.jece.2017.12.028

Shivaprakash, K. N., Ramesh, B. R., Umashaanker, R., and Dayanandan, S. (2018). Functional trait and community phylogenetic analyses reveal environmental filtering as the major determinant of assembly of tropical forest tree communities in the western ghats biodiversity hotspot in india. *Forest Ecosyst.* 5:25. doi: 10.1186/s40663-018-0144-0

Sonia, J., Ocampo-Pérez, R., Mendoza, M. S., Ramos, R., Azuara, A., and Castillo, N. A. (2018). Walnut shell treated with citric acid and its application as biosorbent in the removal of Zn(II). *J. Water Process Eng.* 25, 45–53. doi: 10.1016/j.jwpe.2018.06.007

Srivastava, V., and Sillanpää, M. (2016). Synthesis of malachite@clay nanocomposite for rapid scavenging of cationic and anionic dyes from synthetic wastewater. *J. Environ. Sci.* 51, 97–110. doi: 10.1016/j.jes.2016.08.011

Tarmizi, T., Risfidian, M., Rohendi, D., and Lesbani, A. (2017). "Kinetic and thermodynamic adsorption studies of congo red on bentonite," in *AIP Conference Proceedings* (Yogyakarta: AIP Publishing), 1823, 020028-1–020028-8. doi: 10.1063/1.4978101

Tesfaye, T., Sithole, B., and Ramjugernath, D. (2018). Valorisation of waste chicken feathers: optimisation of decontamination and pre-treatment with bleaching agents using response surface methodology. *Sustain. Chem. Pharma.* 8, 21–37. doi: 10.1016/j.scp.2018.02.003

Tohdee, K., Kaewsichana, L., and Ullah, A. (2018). Enhancement of adsorption efficiency of heavy metal Cu(II) and Zn(II) onto cationic surfactant modified bentonite. *J. Environ. Chem. Eng.* 6, 2821–2828. doi: 10.1016/j.jece.2018.04.030

Toor, M., Jin, B., Dai, S., and Vimonses, V. (2015). Activating natural bentonite as a cost-effective adsorbent for removal of Congo Red in wastewater. *J. Ind. Eng. Chem.* 21, 653–661. doi: 10.1016/j.jiec.2014.03.033

Wang, H., Qin, X. Y., Li, Z. Y., Zheng, Z. Z., and Fan, T. Y. (2018). Preparation and characterization of citric acid-modified superparamagnetic iron oxide nanoparticles. *J. Peking Univ.* 2, 340–346. doi: 10.3969/j.issn.1671-167X.2018.02.023

Wang, Y. Y., Shi, H. Z., Zhang, H. B., Yu, S. M., Chen, N. H., and Tong. Z. F. (2017). Research on Cr(VI) adsorption with magnetic citric acid bentonite. *J. Chem. Eng. Chin. Univ.* 3, 726–732. doi: 10.3969/j.issn.1003-9015.2017.03.030

Wen, Q., Qiong, H., Yi, Z., Jin, P., and Li, Z. (2016). Microwave-assisted regeneration of spent activated carbon containing zinc acetate and its application for removal of Congo Red. *Desalin Water Treat.* 57, 28496–28511. doi: 10.1080/19443994.2016.1179675

Xavier, A., Adarme, O., Furtado, L. M., Ferreira, G., Da, L. S., and Gil, L. F. (2018). Modeling adsorption of Copper(II), Cobalt(II) and Nickel(II) metal ions from aqueous solution onto a new carboxylated sugarcane bagasse. part II: optimization of monocomponent fixed-bed column adsorption. *J. Colloid Interf. Sci.* 516, 431–445. doi: 10.1016/j.jcis.2018.01.068

Xu, L., Xu, X., Cao, G., Liu, S., Duan, Z., Song, S., et al. (2018). Optimization and assessment of Fe-electrocoagulation for the removal of potentially toxic metals from real smelting wastewater. *J. Environ. Manage.* 218, 129–138. doi: 10.1016/j.jenvman.2018.04.049

Xu, Y., Asim, K. M., Wang, F. Y., Xia, M. Z., and Lei, W. (2018). Novel multi amine-containing gemini surfactant modified montmorillonite as adsorbents for removal of phenols. *Appl. Clay Sci.* 162, 204–213. doi: 10.1016/j.clay.2018.06.023

Yan, J., Lan, G., Qiu, H., Chen, C., Liu, Y., and Du, G. (2018). Adsorption of heavy metals and methylene blue from aqueous solution with citric acid modified peach stone. *Sep. Sci. Technol.* 11, 1678–1688. doi: 10.1080/01496395.2018.1439064

Yao, M., Zhang, X., and Lei, L. (2012). Removal of reactive blue 13 from dyeing wastewater by self-assembled organobentonite in a one-steep progress. *J. Chem. Eng. Data* 57, 1915–1922. doi: 10.1021/je300216e

Ye, W., Lin, J., Borrego, R., Chen, D., Sotto, A., Luis, P., et al. (2018). Advanced desalination of dye/NaCl mixures by a loose nanofiltration membrane for digital ink-jet printing. *Sep. Purif. Technol.* 197, 27–35. doi: 10.1016/j.seppur.2017.12.045

Yen, L., Yee, W., Tze, A., Soon, O., Nabilnah, L., and Li, H. (2017). Degradation reaction of diazo reactive black 5 dye with Copper (II) sulfate catalyst in thermolysis treatment. *Environ. Sci. Pollut. Res. Int.* 25, 7067–7075. doi: 10.1007/s11356-017-1069-9

Yin, Z. C., Wang, Y. L., and San, J. S. (2018). Adsorption behavior of hydroxypropyl guar gum onto montmorillonite and reducing adsorption in the reservoir. *Appl. Clay Sci.* 166, 123–130. doi: 10.1016/j.clay.2018.09.015

Zhang, C., Qi, Y. H., Qian, P., Zhong, M. J., Wang, L., and Yin, H. Z. (2014). Quantum chemical study of the adsorption of water molecules on kaolinite surfaces. *Comput. Theor. Chem.* 1046, 10–19. doi: 10.1016/j.comptc.2014.07.004

Zhang, H. B., Tong, Z. F., Wei, T. Y., and Tang, Y. K. (2011). Removal characteristics of Zn(II) from aqueous solution by alkaline Ca-bentonite. *Desalination* 276, 103–108. doi: 10.1016/j.desal.2011.03.026

Zhang, H. B., Zhang, T. S., Tang, Y. K., Wei, T. Y., Tong, Z. F., and Deng, Z. F. (2013). Adsorption of methylene blue and congo red on alkaline Ca-bentonite. *Fine Chem.* 30, 657–673. doi: 10.13550/j.jxhg.2013.06.026

Zhao, J. B., Zou, Z. D., Ren, R., Sui, X. F., Mao, Z. P., Xu, H., et al. (2018). Chitosan adsorbent reinforced with citric acid modified β-cyclodextrin for highly efficient removal of dyes from reactive dyeing effluents. *Eur. Polym. J.* 108, 212–218. doi: 10.1016/j.eurpolymj.2018.08.044

Zhou, J., Zhang, H. B., Tong, Z. F., Qin, Y. L., Chen, G. H., Song, Z. Y., et al. (2015). Adsorption behavior of methylene blue on citric acid bentonite. *Chinese J. Chem. Eng.* 3, 1057–1061.

Zhou, Y., Yao, S., Ma, Y., Li, G., Huo, Q., and Liu, Y. (2018). An anionic single-walled metal-organic nanotube with an armchair (3,3) topology as an extremely smart adsorbent for the effective and selective adsorption of cationic carcinogenic dyes. *Chem. Commun.* 54:3006. doi: 10.1039/C8CC00542G

Conflict of Interest Statement: The authors declare that the research was conducted in the absence of any commercial or financial relationships that could be construed as a potential conflict of interest.